Development and Validation of a Generalized Biaxial Hysteresis Model

Chi-Hsiang Wang, A.M.ASCE[1]; and Shuenn-Yih Chang[2]

Abstract: Biaxial flexural interaction has been known to significantly affect, in many cases magnify, structural response in the inelastic range. Compared to uniaxial cases, the distinct characteristics of biaxial hysteresis curves often observed are negative stiffness and rounded corners of the curves near the time instants of unloading. Developed based on the widely used Bouc-Wen model, this paper presents a generalized biaxial smooth hysteresis model that takes into account the commonly observed hysteretic characteristics of strength and stiffness degradation, asymmetry in ultimate positive and negative forces, pinching, and those exclusively found in biaxial interaction. The capabilities of the developed model are illustrated by comparing the model results to the results of two cyclic and two quasi-static reinforced concrete column tests.

DOI: 10.1061/(ASCE)0733-9399(2007)133:2(141)

CE Database subject headings: Biaxial loads; Earthquake loads; Inelastic action; Hysteresis; Degradation; Dynamic analysis.

Introduction

Lateral load-resisting elements of a structural system under seismic loads are usually subjected to axial force and biaxial bending moments under multidimensional excitations, torsional motion, or when the structure possesses structural irregularity such as stiffness and/or mass eccentricity, irregular layout, and setback. Biaxial flexural interaction has been known to significantly affect, in many cases magnify, the response in the inelastic range from laboratory studies (e.g., Bresler 1960; Aktan and Pecknold 1974; Takizawa and Aoyama 1976; Bousias et al. 1995; Qiu et al. 2002) and field surveys after recent earthquakes; e.g., the 1995 Kobe, Japan (JSCE 1995), and the 1999 Chi-Chi, Taiwan, earthquakes (Wang and Foliente 2000). The magnification of structural response due to biaxial interaction is primarily caused by yielding or damaging of structural elements in one axis that at the same time makes the strength and stiffness in the other axis weakened. Therefore, biaxial hysteresis curves may exhibit markedly different properties from that of uniaxial hysteresis.

Depending on the type of material and configuration of structure, uniaxial hysteresis curves of a system could exhibit phenomena such as stiffness and/or strength degradation, asymmetry in positive and negative yield strengths, and pinching as often observed in reinforced concrete (RC) columns (e.g., Abrams 1987a; Liu 2004), RC beam-column joints (Abrams 1987b), fractured welded steel beam-column joints (Wang and Wen 2000), and timber shearwalls (e.g., Wang and Foliente 2006). In addition to those hysteretic characteristics observed in uniaxial hysteresis, the distinct characteristics of biaxial hysteresis curves that could occur are negative stiffness and roundness of corners near the instances of unloading (Bousias et al. 1995; Qiu et al. 2002).

While many uniaxial hysteresis models have been developed for plane frame analysis, only a limited number of models exist for biaxial hysteresis. Aktan and Pecknold (1974) and Suharwardy and Pecknold (1978) extended the uniaxial fiber theory to model the behavior of RC columns under bidirectional earthquake shaking. Similarly, Takizawa and Aoyama (1976) extended a uniaxial trilinear hysteresis model for RC columns, which uses one inner and one outer failure ellipse for concrete cracking and member yielding, respectively, to account for biaxial bending. Inelastic behavior in this model is dictated by the stress-strain characteristics of concrete and reinforcing steel. Lai and Will (1986) proposed a triaxial spring model that consists of a linearly elastic line element between two inelastic elements at the two ends of a RC member. Each inelastic element comprises four steel spring elements and five effective concrete spring elements. The Lai and Will (1986) model is able to count for axial force-biaxial bending interaction, stiffness degradation, strength asymmetry, and pinching. Park et al. (1986) generalized the original Bouc-Wen model (Wen 1976), expressed in the form of differential equation, for random vibration analysis of RC members under bidirectional ground motions even though this model applies equally well for time history analysis. The Park et al. (1986) model was subsequently adapted by Kunnath and Reinhorn (1990), where the stiffness degradation is modeled by an exponential function of the member ductility and the strength deterioration is approximated as a linear function of cumulative dissipated energy. Marante and Flórez-López (2002, 2003) combined the concepts of fracture mechanics, continuum damage mechanics, plastic hinge, and axial-flexural interaction surface, of which the yield loci are governed by the kinematic hardening rules of plasticity theory, to proposing a framework called lumped damage mechanics that considers the effects of axial, flexural, and

[1]Senior Research Scientist, CSIRO Division of Sustainable Ecosystems, P.O. Box 56, Highett, Victoria 3190, Australia; formerly, Research Scientist and Project Leader, CSIRO Division of Manufacturing and Infrastructure Technology. E-mail: Chi-hsiang.Wang@csiro.au

[2]Professor, Dept. of Civil Engineering, National Taipei Univ. of Technology, 1 Sec. 3, Jungshiau E. Rd., Taipei 106-08, Taiwan. E-mail: changsy@ntut.edu.tw

Note. Associate Editor: George Z. Voyiadjis. Discussion open until July 1, 2007. Separate discussions must be submitted for individual papers. To extend the closing date by one month, a written request must be filed with the ASCE Managing Editor. The manuscript for this paper was submitted for review and possible publication on October 24, 2005; approved on July 17, 2006. This paper is part of the ***Journal of Engineering Mechanics***, Vol. 133, No. 2, February 1, 2007. ©ASCE, ISSN 0733-9399/2007/2-141–152/$25.00.

torsional forces for spatial analysis of RC frames. Developed for modeling thin-walled circular steel columns, Goto et al. (1998) used shell elements in nonlinear finite element analysis and later revised it to a multispring model (Jiang et al. 2002). This spring model is similar in idea to the fiber model, but the ends of the column are modeled by springs, whose hysteretic behavior of springs is governed by a modified bounding-line theory, and the whole segment between the two ends is assumed to be a rigid body. El-Tawil and Deierlein (2001a,b), making use of the flexibility method and bounding surface plasticity model, developed a plasticity-based distributed beam-column element model intended for analysis of steel, RC, and composite beam columns.

In general, the existing models can be classified into two broad categories: The first is based on fiber theory (Aktan and Pecknold 1974; Suharwardy and Pecknold 1978; Goto et al. 1998; El-Tawil and Deierlein 2001a,b; Jiang et al. 2002), which typically discretizes the cross section of a structural member into fibers of finite length and in series along the member; each of the fibers has the uniaxial constitutive properties of the member. A fiber-theory model generally allows the spread of yielding over a finite length of the member. The second category uses the concept of plastic hinges (Takizawa and Aoyama 1976; Lai and Will 1986; Park et al. 1986; Kunnath and Reinhorn (1990); Marante and Flórez-López 2002) which lumps the inelastic behavior to localized regions, e.g., the two ends of the member. Typically, a model using the fiber theory is more versatile and may be applicable to a variety of structural elements, but much more demanding in computation than localized plasticity models. Of the models reviewed, however, only the models by Lai and Will (1986), and El-Tawil and Deierlein (2001a) considers pinching phenomenon that could cause amplification in displacement demand (e.g., Mostaghel 1999; Paevere and Foliente 2000). On the other hand, only the model by Park et al. (1986) captures the smooth, rounded corners of hysteresis curves. The dissipated hysteretic energy, estimated by the enclosed areas of hysteresis curves, is often used as a performance indicator of inelastic systems under dynamic loads. As a result, negligence of rounded corners in the force-displacement relations, if manifested prominently, may lead to unwarranted underestimation of dissipated energy, as will be shown later in Fig. 6 in the model validation section.

The smooth hysteresis model by Park et al. (1986), expressed as a pair of coupled nonlinear differential equations, is easy to implement and is efficient in computation yet versatile enough to account for most of the hysteretic characteristics except strength asymmetry and pinching. On the basis of this model, therefore, this paper proposes a generalized biaxial smooth hysteresis model that is capable of simulating strength asymmetry and pinching phenomena as well.

In the following, a modified uniaxial Bouc-Wen model (Wen 1976) that accounts for strength asymmetry is first presented. Generalization of the asymmetric uniaxial model to its biaxial counterpart is then described, followed by consideration of the pinching mechanism. Calculation of dissipated hysteretic energy, stiffness, and strength degradation is also presented. The developed model is validated by comparing the model results to the results of two cyclic and two quasi-static reinforced concrete column tests.

Uniaxial Hysteresis Model

For a single-degree-of-freedom system of mass m subjected to ground acceleration $\ddot{u}_g$ the equation of motion neglecting viscous damping is

$$m\ddot{u}(t) + q(t) = -m\ddot{u}_g(t) \tag{1}$$

in which t=time; the dots overhead denote the derivatives with time; and the restoring force q may be decomposed into two components, one elastic and one hysteretic, as follows:

$$q(t) = \alpha k u(t) + (1-\alpha)kz(t) \tag{2}$$

where u=displacement of the system; k=initial stiffness; α=ratio of stiffness before yielding to that after yielding; and z=internal variable proportional to the hysteretic restoring force.

While the original Bouc-Wen model (Wen 1976) is versatile and easy to apply, the main disadvantage is that some of its parameters lack physical significance, making it difficult to obtain good initial guessed values of the parameters. Besides, it does not consider pinching phenomenon and strength asymmetry. Baber and Noori (1985) proposed a slip-lock element that was modeled by a bell-shaped function, specifically the family of normal distribution functions, for pinching. Wang and Wen (2000) added another parameter to account for strength asymmetry. However, lack of physical meaning in parameters still remained. Ways to overcome this and eliminate redundant parameters were investigated by Ma et al. (2004). In light of these, a modified Bouc-Wen model accounting for strength asymmetry could be expressed as

$$\dot{z}(t) = \frac{\dot{u}(t)}{\eta(t)} h(t) \tag{3}$$

where

$$h(t) = 1 - \left| \frac{z(t)}{z_u(t)} \right|^n (1 + \beta\{\mathrm{sgn}[\dot{u}(t)z(t)] - 1\}) \tag{4}$$

in which sgn $(\cdot)$=signum function; the parameter n, taken as an integer, determines the sharpness of the hysteresis before yielding (the larger the n value, the more it resembles a bilinear hysteresis); η dictates stiffness degradation (η=1 means no degradation); β=parameter controlling the unloading shape of the hysteresis (when $0<\beta<0.5$, the hysteresis loop takes a slim S shape; when $\beta=0.5$, it exhibits linear unloading; when $\beta>0.5$, it takes a bulge shape). z_u is the instantaneous ultimate value of the internal variable z determined by

$$z_u(t) = \frac{1}{2\nu(t)} (\{1 + \mathrm{sgn}[z(t)]\}|z_{u0}^+| + \{1 - \mathrm{sgn}[z(t)]\}|z_{u0}^-|) \tag{5}$$

in which ν=parameter controlling strength deterioration (ν=1 means no degradation); numerically z_{u0}^+ and z_{u0}^- represent the initial positive and negative yield displacements, respectively. Thus Eq. (5) accounts for the asymmetry and deterioration of yield strength.

The main advantage of the revised Bouc-Wen model expressed in Eqs. (3) to (5) is that it consists of six model parameters $(n, \eta, \beta, \nu, z_{u0}^+, z_{u0}^-)$ instead of eight used in Wang and Wen (2000); in addition, the parameters are physically meaningful. System parameter identification, therefore, is easier for the revised model.

The slip behavior observed in a pinching hysteresis, as discussed by Baber and Noori (1985), can be approximated by a slip-lock element. The following function is used in this study:

Table 1. Parameter Values for Uniaxial, Asymmetric, Nondegrading Hysteretic System

f_y^+	f_y^-	k	n	β	η	ν	s	μ	σ
100	85	10	10	0.5	1	1	1	0.1	0.1

$$p(t) = \sqrt{\frac{2}{\pi}}\frac{s(t)}{\sigma}\exp\left\{-\frac{1}{2}\left[\frac{\mathrm{sgn}[\dot{u}(t)]\dfrac{z(t)}{z_u(t)} - \mu}{\sigma}\right]^2\right\} \tag{6}$$

in which the parameter s controls the length (or spread) of slip ($s=0$ means no pinching); σ controls the sharpness of pinching (i.e., a smaller σ value gives a flatter pinching region); μ denotes the fraction of z_u at which the stiffness reaches the minimum, thus controlling the "thickness" of pinching area. The smooth uniaxial hysteresis model considering stiffness and strength degradation, asymmetry, and pinching is derived as follows:

$$\dot{z}(t) = \frac{h(t)}{\eta(t) + p(t)h(t)}\dot{u}(t) \tag{7}$$

Detailed derivation of Eq. (7) can be found in Wang and Wen (2000).

To see the effect and physical significance of pinching parameters, consider a nondegrading system with values of the hysteretic parameters listed in Table 1. The system is subjected to an incremental displacement history of sine function, $u(x)=30\sin(3\pi x), x=0, 0.002, \ldots, 1$.

The displacement u may be treated as the superposition of two components (Wang and Wen 2000): One that contributes to hysteretic energy dissipation u_1 and the other to the spread of pinching u_2. The decomposed and resultant hysteresis curves are shown in Fig. 1. Fig. 1(a) shows contribution from the displacement other than slippage, Fig. 1(b) from that by slippage, and Fig. 1(c) is the resultant hysteresis. From Figs. 1(b and c), one can see that the "thickness" of the pinching region is $\mu\times(f_y^+ + f_y^-)=18.5$, where f_y^+ and f_y^- are the yield forces in positive and negative directions, respectively. The slip length is $s\times(z_u^+ + z_u^-)=18.5$, where $z_u^\pm = f_y^\pm/k$, and k is the initial stiffness. The "sharpness" of pinching, i.e., the force span in a region that undergoes about a full slip length, is approximately equal to $\sigma\times(f_y^+ + f_y^-)=18.5$.

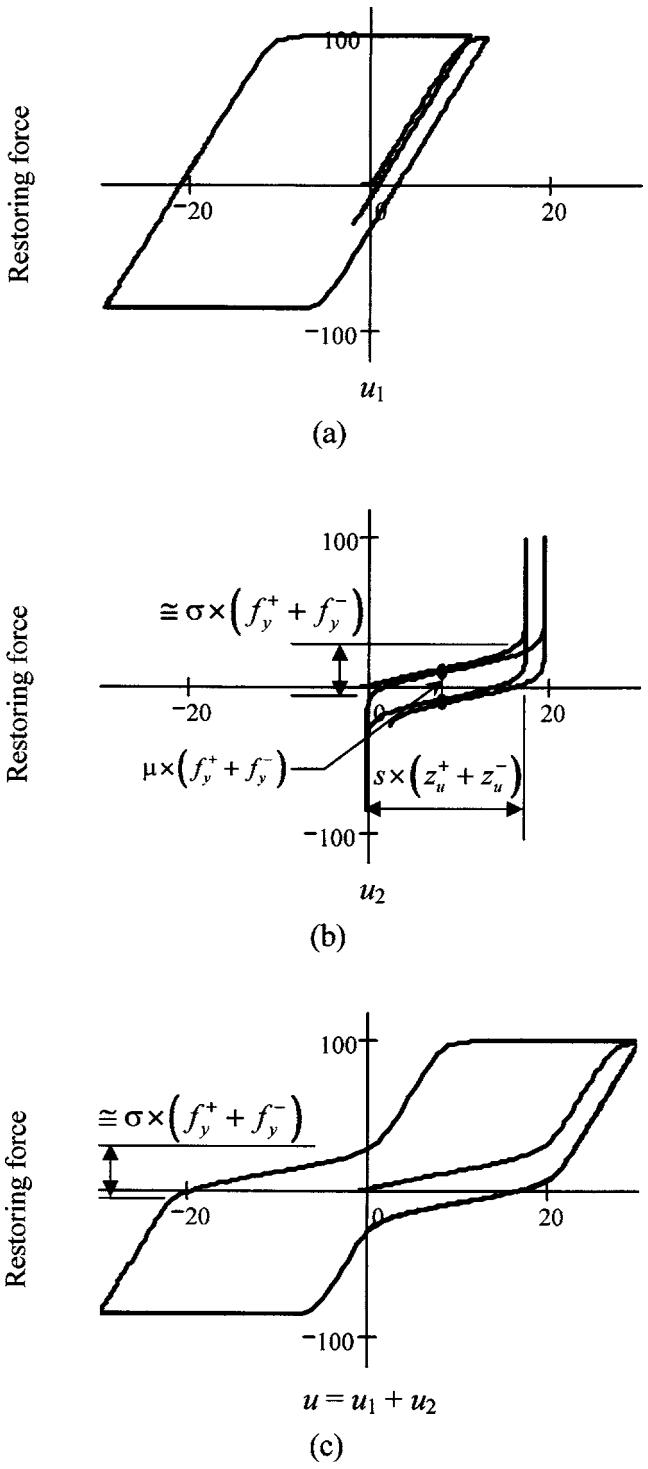

Fig. 1. Decomposed and resultant hysteresis: (a) hysteretic component without pinching; (b) slippage due to slip-lock element; and (c) resultant pinching hysteresis

Biaxial Hysteresis without Pinching

The undamped equations of motion of a two-degrees-of-freedom inelastic system of mass m subjected to bidirectional excitations $\ddot{u}_{gx}$ and $\ddot{u}_{gy}$ in the two orthogonal directions x and y are

$$m\ddot{u}_x + q_x = -m\ddot{u}_{gx}; \quad m\ddot{u}_y + q_y = -m\ddot{u}_{gy} \tag{8}$$

where u_x, u_y, and q_x, q_y=displacements and restoring forces along the x and y directions. As discussed in Park et al. (1986), when the system is orthotropic, the restoring forces are expressed as

$$\begin{aligned} q_x &= \alpha_x k_x u_x + (1-\alpha_x)k_x z_x = q_{ux} + q_{zx} \\ q_y &= \alpha_y k_y u_y + (1-\alpha_y)k_y z_y = q_{uy} + q_{zy} \end{aligned} \tag{9}$$

where z_x and z_y=internal variables related to the restoring forces along the x and y directions, respectively; k_x, k_y=initial stiffness and α_x, α_y=post-to-pre-yielding stiffness ratio; q_{ux}, q_{uy}, and q_{zx}, q_{zy} denotes, respectively, the elastic and hysteretic restoring-force components. If coordinate transformation is applied, the orthotropic system can be transformed into an equivalent isotropic system. For instance, if the displacement and hysteretic restoring force in the y direction are transformed by

$$u_y' = \frac{z_{ux0}^+}{z_{uy0}^+}u_y; \quad q_{zy}' = \frac{(1-\alpha_x)k_x z_{ux0}^+}{(1-\alpha_y)k_y z_{uy0}^+}q_{zy} \tag{10}$$

in which u_y'=transformed displacement and q_{zy}'=transformed hysteretic force; z_{ux0}^+ and z_{uy0}^+=initial positive yield displacements in the x and y axes, respectively, then the restoring forces, when

expressed in the original coordinate system, become (Park et al. 1986)

$$q_x = \alpha_x k_x u_x + (1-\alpha_x) k_y z_x'; \quad q_y = \alpha_y k_y u_y + (1-\alpha_y)\frac{z_{uy0}^+}{z_{ux0}^+} k_y z_y' \tag{11}$$

In the transformed coordinates, the instantaneous yield displacements are $z_u(t)=z_{ux}(t)=z_{uy}'(t)$. Therefore,

$$z_u(t) = \frac{\{1+\text{sgn}[z_x'(t)]\}|z_{ux0}^+| + \{1-\text{sgn}[z_x'(t)]\}|z_{ux0}^-|}{2\nu(t)} \tag{12}$$

in which z_{ux0}^- denotes the initial negative yield displacement in x. z_x' and z_y' must satisfy the following coupled nonlinear differential equations:

$$\dot{z}_x' = \frac{1}{\eta}\left(\dot{u}_x - \frac{z_x'}{z_u} I_b\right); \quad \dot{z}_y' = \frac{1}{\eta}\left(\frac{z_{ux0}^+}{z_{uy0}^+}\dot{u}_y - \frac{z_y'}{z_u} I_b\right) \tag{13}$$

in which I_b is a function accounting for the effect of biaxial interaction

$$I_b = \dot{u}_x \frac{z_x'}{z_u}\{1+\beta[\text{sgn}(\dot{u}_x z_x')-1]\} + \dot{u}_y \frac{z_{ux0}^+}{z_{uy0}^+}\frac{z_y'}{z_u}\{1+\beta[\text{sgn}(\dot{u}_y z_y')-1]\} \tag{14}$$

Note that for asymmetric hysteresis this model is applied only to cases in which the x and y axes have the same ratio of asymmetry; i.e., $f_{yx}^+/f_{yx}^- = f_{yy}^+/f_{yy}^-$, due to the isotropic transformation of the system.

Biaxial Hysteresis with Pinching

Similar to the uniaxial hysteresis, if the displacement in one direction is considered as the superposition of one component contributing to hysteretic energy dissipation and the other to the spread of pinching; i.e.,

$$\dot{u}_x = \dot{u}_{x1} + \dot{u}_{x2}; \quad \dot{u}_y = \dot{u}_{y1} + \dot{u}_{y2} \tag{15}$$

in which u_{x1} and u_{y1}=components contributing to energy dissipation. They are related to z_x' and z_y' by

$$\dot{z}_x' = \frac{1}{\eta}\left(\dot{u}_{x1} - \frac{z_x'}{z_u} I_{bp}\right); \quad \dot{z}_y' = \frac{1}{\eta}\left(\frac{z_{ux0}^+}{z_{uy0}^+}\dot{u}_{y1} - \frac{z_y'}{z_u} I_{bp}\right) \tag{16}$$

where

$$I_{bp} = \dot{u}_{x1}\frac{z_x'}{z_u}\{1+\beta[\text{sgn}(\dot{u}_{x1} z_x')-1]\} + \dot{u}_{y1}\frac{z_{ux0}^+}{z_{uy0}^+}\frac{z_y'}{z_u}\{1+\beta[\text{sgn}(\dot{u}_{y1} z_y')-1]\} \tag{17}$$

If a pair of slip-lock functions $p_x(z_x')$ and $p_y(z_y')$ are used

$$p_x(z_x') = \sqrt{\frac{2}{\pi}}\frac{s}{\sigma}\exp\left\{-\frac{1}{2}\left[\frac{\text{sgn}(\dot{u}_x)\frac{z_x'}{z_u}-\mu}{\sigma}\right]^2\right\};$$
$$p_y(z_y') = \sqrt{\frac{2}{\pi}}\frac{s}{\sigma}\exp\left\{-\frac{1}{2}\left[\frac{\text{sgn}(\dot{u}_y)\frac{z_y'}{z_u}-\mu}{\sigma}\right]^2\right\} \tag{18}$$

then the displacements u_{x2} and u_{y2}, caused by the slippage of pinching, are related to z_x' and z_y' as follows:

$$\dot{u}_{x2} = p_x(z_x')\dot{z}_x'; \quad \dot{u}_{y2} = \frac{z_{uy0}^+}{z_{ux0}^+} p_y(z_y')\dot{z}_y' \tag{19}$$

Eq. (15) becomes

$$\dot{u}_{x1} = \dot{u}_x - p_x\dot{z}_x'; \quad \dot{u}_{y1} = \dot{u}_y - \frac{z_{uy0}^+}{z_{ux0}^+} p_y \dot{z}_y' \tag{20}$$

Note that

$$\text{sgn}(\dot{u}_x) = \text{sgn}(\dot{u}_{x1}) = \text{sgn}(\dot{u}_{x2}); \quad \text{sgn}(\dot{u}_y) = \text{sgn}(\dot{u}_{y1}) = \text{sgn}(\dot{u}_{y2}) \tag{21}$$

Substituting Eqs. (20) and (21) into Eq. (17) yields

$$I_{bp} = (\dot{u}_x - p_x\dot{z}_x')\frac{z_x'}{z_u}\{1+\beta[\text{sgn}(\dot{u}_x z_x')-1]\} + \left(\frac{z_{ux0}^+}{z_{uy0}^+}\dot{u}_y - p_y\dot{z}_y'\right)\frac{z_y'}{z_u}\{1+\beta[\text{sgn}(\dot{u}_y z_y')-1]\} \tag{22}$$

Define C_x and C_y as

$$C_x = \frac{z_x'}{z_u}\{1+\beta[\text{sgn}(\dot{u}_x z_x')-1]\}; \quad C_y = \frac{z_y'}{z_u}\{1+\beta[\text{sgn}(\dot{u}_y z_y')-1]\} \tag{23}$$

Then Eq. (16) can be rewritten as

$$\begin{cases} \eta\dot{z}_x' = \dot{u}_x - p_x\dot{z}_x' - \dfrac{z_x'}{z_u}\left[(\dot{u}_x - p_x\dot{z}_x')C_x + \left(\dfrac{z_{ux0}^+}{z_{uy0}^+}\dot{u}_y - p_y\dot{z}_y'\right)C_y\right] \\ \eta\dot{z}_y' = \left(\dfrac{z_{ux0}^+}{z_{uy0}^+}\dot{u}_y - p_y\dot{z}_y'\right) - \dfrac{z_y'}{z_u}\left[(\dot{u}_x - p_x\dot{z}_x')C_x + \left(\dfrac{z_{ux0}^+}{z_{uy0}^+}\dot{u}_y - p_y\dot{z}_y'\right)C_y\right] \end{cases} \tag{24}$$

Collecting terms in Eq. (24) for $\dot{z}_x'$ and $\dot{z}_y'$, and expressing in matrix form lead to

$$\begin{bmatrix} H_{11} & H_{12} \\ H_{21} & H_{22} \end{bmatrix}\begin{Bmatrix} \dot{z}_x' \\ \dot{z}_y' \end{Bmatrix} = \begin{Bmatrix} G_1 \\ G_2 \end{Bmatrix} \tag{25}$$

in which the elements of the coefficient matrix are

$$H_{11} = \eta + \left(1 - \frac{z_x'}{z_u}C_x\right)p_x; \quad H_{12} = -\frac{z_x'}{z_u}C_y p_y;$$
$$H_{21} = -\frac{z_y'}{z_u}C_x p_x; \quad H_{22} = \eta + \left(1 - \frac{z_y'}{z_u}C_y\right)p_y \tag{26}$$

and that of the right-hand side vector are

$$G_1 = \left(1 - \frac{z_x'}{z_u}C_x\right)\dot{u}_x - \frac{z_x'}{z_u}\frac{z_{ux0}^+}{z_{uy0}^+}C_y\dot{u}_y;$$
$$G_2 = -\frac{z_y'}{z_u}C_x\dot{u}_x + \left(1 - \frac{z_y'}{z_u}C_y\right)\frac{z_{ux0}^+}{z_{uy0}^+}\dot{u}_y \tag{27}$$

Then the biaxial hysteresis model may be written as

$$\begin{Bmatrix} \dot{z}_x' \\ \dot{z}_y' \end{Bmatrix} = \frac{1}{H_{11}H_{22} - H_{12}H_{21}}\begin{Bmatrix} H_{22}G_1 - H_{12}G_2 \\ -H_{21}G_1 + H_{11}G_2 \end{Bmatrix} \tag{28}$$

Eqs. (28) and (8) may be solved in tandem by any efficacious first-order differential equation solver, e.g., adaptive step-size Runge-Kutta or Rosenbrock method (Press et al. 1992). Imple-

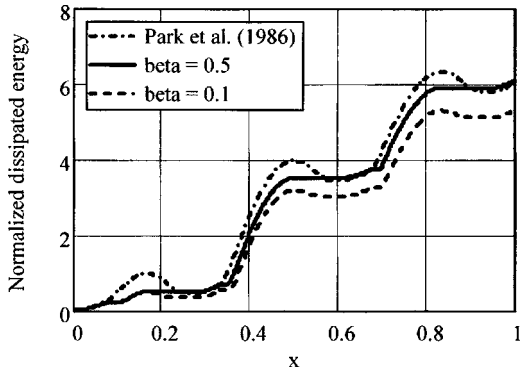

Fig. 2. Computed cumulative energy dissipation

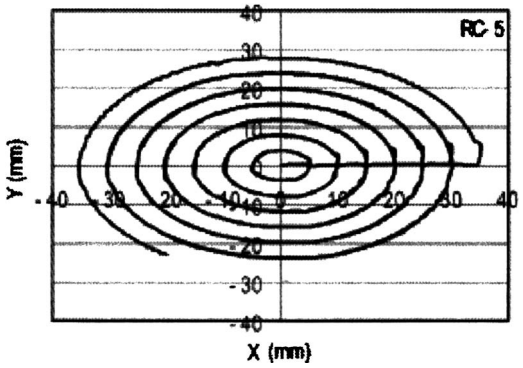

Fig. 3. Displacement path for test RC-5 (Qiu et al. 2002, with permission from Elsevier)

mentation of the model in time history analysis of multidegrees-of-freedom systems is essentially the same as that of the Park et al. (1986) model and can be found elsewhere (e.g., Wen and Yeh 1989; Wang and Wen 1998a, 1998b).

Note that the current form of the developed model does not take into account the effect of axial-flexural interaction, as typical of the family of Bouc-Wen hysteresis models (e.g., Wen 1976; Park et al. 1986; Kunnath and Reinhorn 1990; Sivaselvan and Reinhorn 2000; Ma et al. 2004). When torsion and transverse shear are not considered, the axial-flexural interaction that often causes a reduction in the yield moment capacities may be accounted for by using an appropriate three-dimensional yield surface, which is constructed with one axis representing the axial force and the other two axes the bending moments (e.g., Zahn et al. 1989; McGuire et al. 2000; Furlong et al. 2004). When the axial force varies with time, however, the moment-curvature-axial load relationship becomes highly complicated due to independent loading reversal of bending moments and axial force, which is still a topic of research (Cheng 2001).

Consideration of $P-\Delta$ Effect

For the case of a column, of length l, subjected to an axial force W in addition to lateral forces, the stiffness in the two orthogonal lateral directions may be modified as follows to take into account the $P-\Delta$ effect (Wilson and Habibullah 1987):

$$k_{x,\text{eff}} = k_x - \frac{W}{l}; \quad k_{y,\text{eff}} = k_y - \frac{W}{l} \tag{29}$$

Extension of Eq. (29) to the treatment of $P-\Delta$ effect for multistory building structures can be found in Wilson and Habibullah (1987), and Wang and Wen (1998b). In effect, Eq. (29) accounts for the first-order effect only; i.e., axial displacement and geometric nonlinearity because of excessive lateral displacement are neglected. In the cases where failure is dominated by flexure, this approximate approach may suffice; otherwise, more detailed methods need to be employed to include the second-order effect (e.g., Yang and Kuo 1994; McGuire et al. 2000; Cheng 2001).

Degradation Parameters

In the hysteresis model, the parameters η and ν, respectively, control the deterioration of stiffness and strength of the system, whereas s, μ, and σ control the spread, thickness, and sharpness, respectively, of pinching. For deteriorating systems, η, ν, and s vary with time characterizing the extent of structural damage and are assumed to be functions of a cumulative damage measure D

$$\eta = \eta_0 + \delta_\eta D; \quad \nu = \nu_0 + \delta_\nu D; \quad s = s_0 + \delta_s D \tag{30}$$

where η_0, ν_0, and a_0=initial values; δ_η, δ_ν, and δ_s=rates of degradation. D could be any appropriate damage measure that correlates with system deterioration; for instance, maximum displacement, cumulative dissipated energy, or damage index accounting for both displacement and energy dissipation are among the most often used (e.g., Fajfar 1992).

When dissipated energy is used as a damage parameter, often the normalized cumulative hysteretic energy, denoted by E_η, with respect to elastic strain energy up to yielding is used for this purpose. For hysteresis curves generated by the developed biaxial model, E_η could be evaluated as follows:

$$E_\eta(t) = \frac{(1-\alpha_x)}{2}\int_0^1 \frac{1}{z_u^2}\left[z_x'(\dot{u}_x - \eta\dot{z}_x') + z_y'\left(\frac{z_{ux0}^+}{z_{uy0}^+}\dot{u}_y - \eta\dot{z}_y'\right)\right]dt \tag{31}$$

Eq. (31) is an improvement for the computation of E_η given in Park et al. (1986), which gives nonmonotonic energy dissipation when subject to cyclic loading. For $\beta \geq 0.5$ (linear unloading and bulge-shaped hysteresis), which is true for most practical applications in structural engineering, Eq. (31) gives effectively monotonic increase in dissipated energy, but not for $\beta < 0.5$ (slim-shaped hysteresis). Fig. 2 plots the cumulative energy dissipation

Table 2. Model Parameter Values for Simulation of Test Results

Test	k_x (kN/mm)	k_y (kN/mm)	f_{yx}^+ (kN)	f_{yx}^- (kN)	f_{yy}^+ (kN)	f_{yy}^- (kN)	α_x	α_y	β	η_0	ν_0	δ_η	δ_ν	S_0	δ_s	σ	μ
RC-5	20	20	80	80	80	80	0.02	0.02	0.7	1.0	1.0	0.4	0.05	0.0	0.0	—	—
Cyclic	12.5	8.8	680	680	600	600	0.0	0.0	0.6	1.0	1.0	0.1	0.08	0.0	0.22	0.15	0.3
TCU075	11.0	8.0	550	650	440	520	0.05	0.05	0.8	1.0	1.0	0.07	0.0	0.25	0.1	0.3	0.06
TCU102	14.5	7.2	550	605	420	462	0.05	0.01	1.2	1.0	1.0	0.2	0.02	0.3	0.04	0.15	0.07

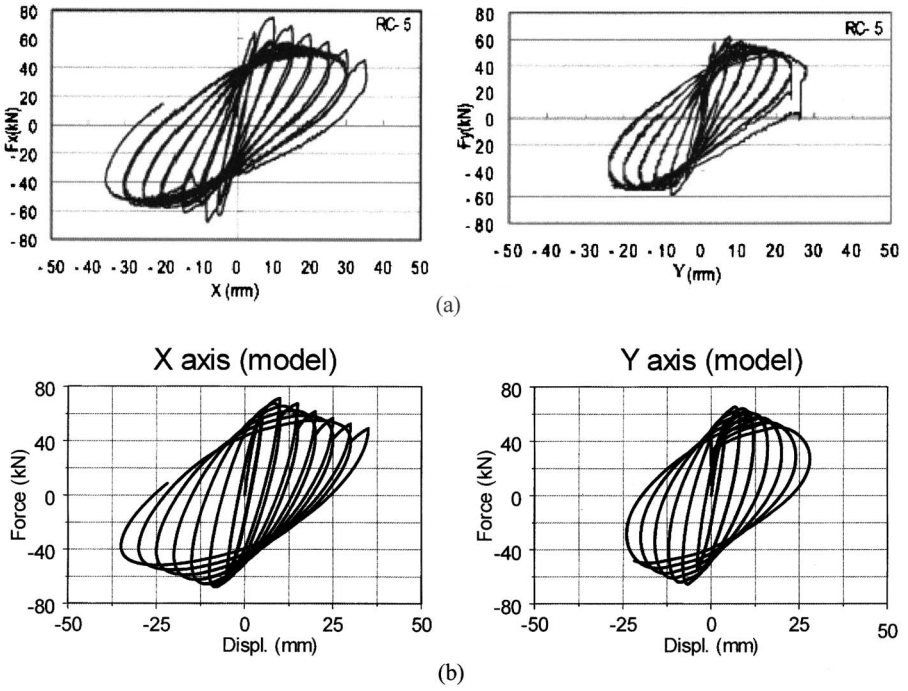

Fig. 4. Hysteresis curves for RC-5 test by Qiu et al. (2002): (a) test result (with permission from Elsevier); (b) model result

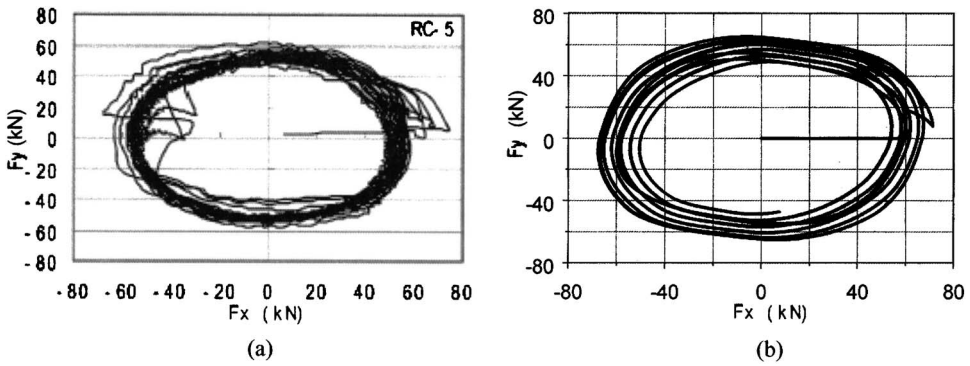

Fig. 5. Force-path orbit for RC-5 test by Qiu et al. (2002): (a) test result (with permission from Elsevier); (b) model result

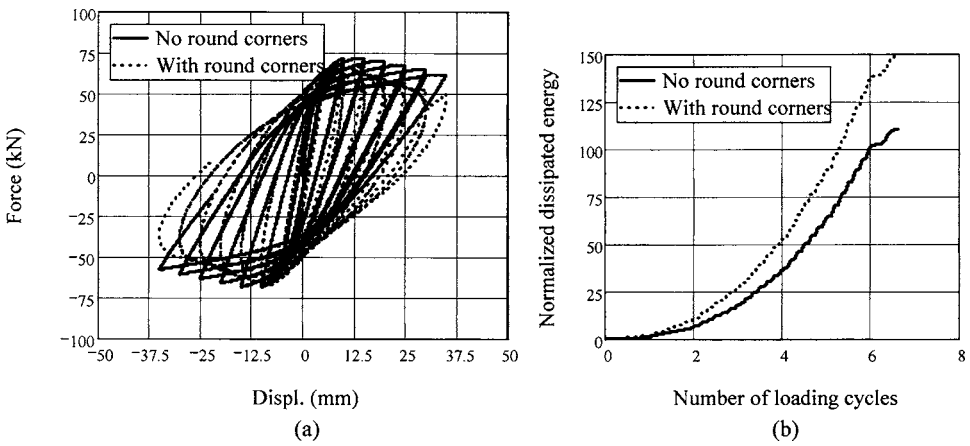

Fig. 6. Comparison of hysteresis with and without round corners: (a) hysteresis curves; (b) normalized dissipated energy

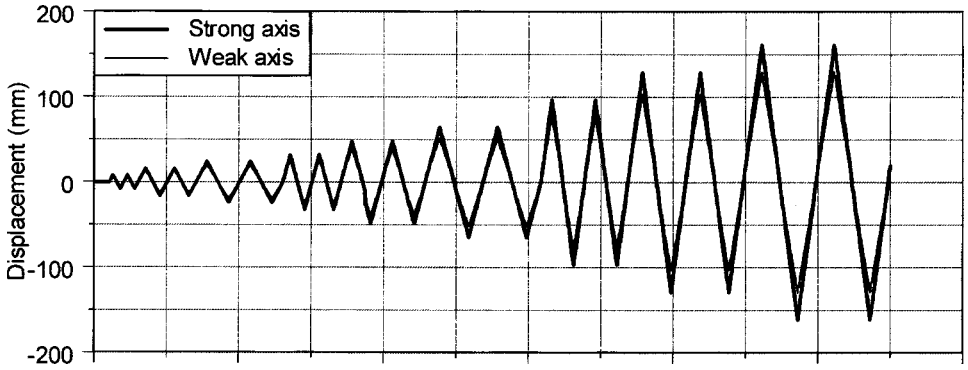

Fig. 7. Displacement history for cyclic test (Liu 2004)

by using Park et al. (1986) for $\beta=0.5$, as well as that by Eq. (31) for $\beta=0.5$ and $\beta=0.1$, for the simple system discussed in the section of uniaxial hysteresis model. It can be seen in Fig. 2 that the energy dissipation by Park et al. (1986) and for $\beta=0.1$ by Eq. (31) are not monotonic. A more comprehensive treatment of non-decreasing energy dissipation is found in Bockstedte (1999).

If both displacement and energy dissipation are taken into account, a commonly used damage index is the Park-Ang damage index (Park and Ang 1985). For biaxial hysteresis, it may be written as follows for the two axes x and y:

$$I_{Dx}(t)=\frac{u_{\max,x}(t)}{z_{ux0}}+\lambda E_n(t);\quad I_{Dy}(t)=\frac{u_{\max,y}(t)}{z_{uy0}}+\lambda E_n(t) \quad (32)$$

where $u_{\max,x}$ and $u_{\max,y}$=maximum displacements experienced up to the time instant t, and λ=parameter accounting for damage contribution of the dissipated energy. Hence when $\lambda=0$, Eq. (32) reduces to a damage measure dependent only on the maximum displacement experienced.

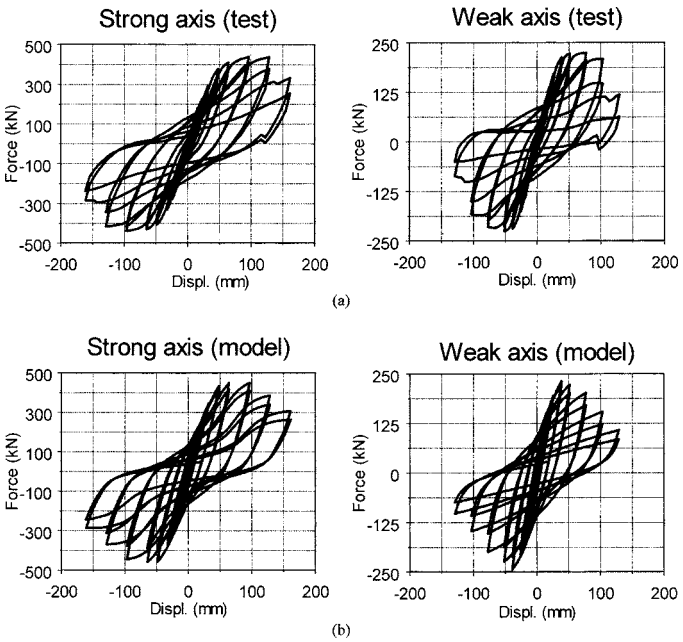

Fig. 8. Hysteresis curves for cyclic test by Liu (2004): (a) test result; (b) model result

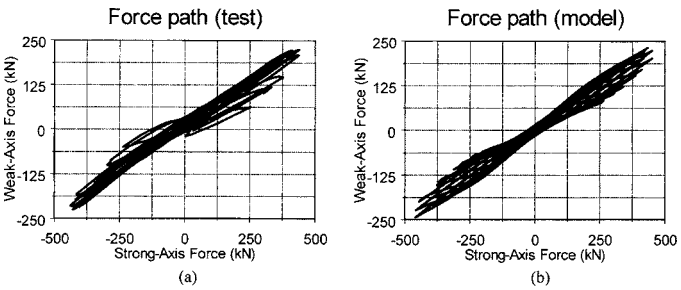

Fig. 9. Force-path orbit for cyclic test by Liu (2004): (a) test result; (b) model result

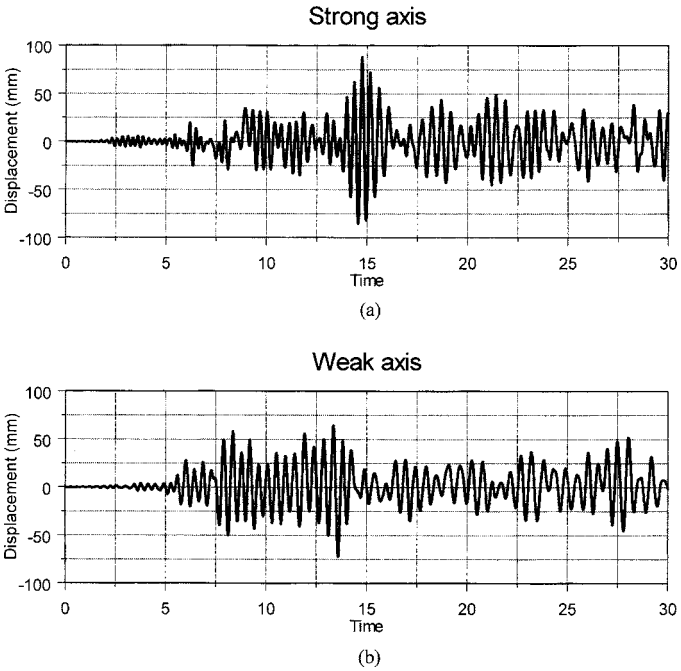

Fig. 10. Pseudodynamic input displacement history using TCU075: (a) strong axis; (b) weak axis

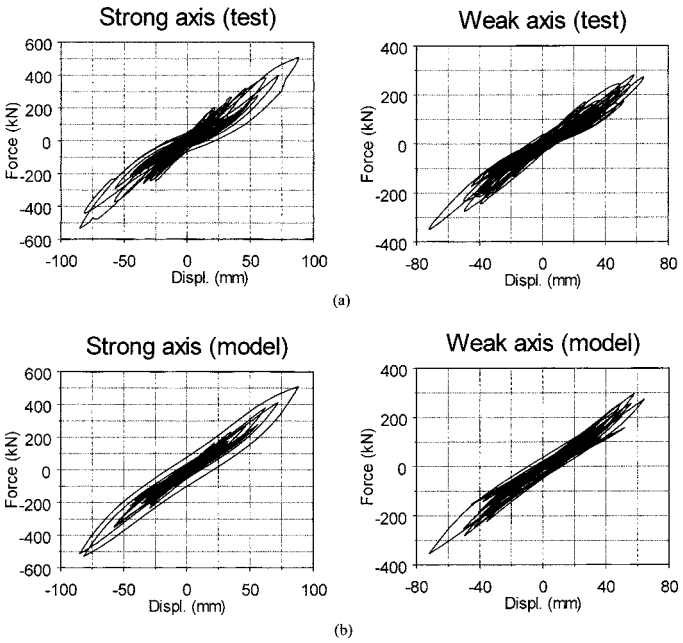

Fig. 11. Hysteresis curves under TCU075: (a) test result; (b) model result

Model Validation

As illustrations for the validity of the developed model, hysteretic behavior of four reinforced concrete columns is examined. One is from the test specimen RC-5 investigated by Qiu et al. (2002); the other three are from the tests documented in Liu (2004).

The specimen tested by Qiu et al. (2002) had a 200 $\times$ 200 mm square cross section and a free length of 960 mm. The longitudinal reinforcement (8 $\phi-12$ mm) was uniformly distributed around the perimeter of the section and $\phi-6$ mm transverse reinforcing bars at 50 mm. The compressive strength of the concrete was 38.2 MPa.

The three specimens used in Liu (2004) were identical in nominal dimensions and nominal material strengths. They were 40% scaled-down versions of a full-sized column designed in accordance with the 1995 Taiwan Bridge Design Code. They had a nominal cross section of 750 $\times$ 600 mm and a height of 3,250 mm. The average yield strengths of longitudinal reinforcing bars (32 $\phi-19$ mm in each specimen) and the confining stirrups ($\phi-10$ mm at 100 mm) were determined to be 520 and 400 MPa, respectively. Concrete cylinders had an average 28-day compressive strength of 25 MPa. One specimen was used for displacement-controlled cyclic test and the other two were subjected to quasi-static tests.

Since each of the system and hysteretic parameters has a clear physical meaning, visual inspection together with trial and error may be sufficient to obtain satisfactory parameter values, as was done for the results presented below. Alternatively, system identification or functional optimization methods such as downhill Simplex, simulated annealing (e.g., Press et al. 1992), and fast Bayesian Bootstrap filter (Li et al. 2004) could be employed for this task. The identified model parameters for the four simulated results are tabulated in Table 2. Comparison of the test and model results is presented in the following.

Displacement-Controlled Cyclic Tests

The test specimen RC-5 conducted by Qiu et al. (2002) was subjected to elliptic deflection paths, which consisted of three cycles at each of the seven successive ellipses with major axes of $10,20,30,\ldots,70$ mm, and minor axes of $8,16,24,\ldots,56$ mm, as shown in Fig. 3. A constant axial load equal to 360 kN was applied throughout the testing. Damage condition at the end of the test was unknown as it was not documented in Qiu et al. (2002).

The most obvious hysteretic characteristics of this test are the round corners, the almost linear degradation in strength as well as stiffness, and the three cycles of the same amplitude virtually overlapping, as revealed in Fig. 4(a). Therefore, the damage index, Eq. (32), is used as the damage measure with $\lambda=0$, meaning that degradation is totally due to the maximum displacement experienced. The simulated hysteresis curves are plotted in Fig. 4(b). The force-path orbits from the test and model results are shown in Fig. 5. It is seen that the modeled hysteresis captures all the hysteretic characteristics of the test results.

The manifestation of rounded corners in a hysteresis curve, if as prominent as that seen in Fig. 4, may have significant consequences on energy dissipation. For instance, Fig. 6(a) shows the hysteretic response by Qiu et al. (2002) in the x axis with and without round corners, and Fig. 6(b) compares the energy dissipated in the two hysteresis curves. It is revealed in this case that when round corners are neglected, the force-displacement relation becomes progressively inaccurate and the dissipated energy at the end of the test is underestimated by about 25%.

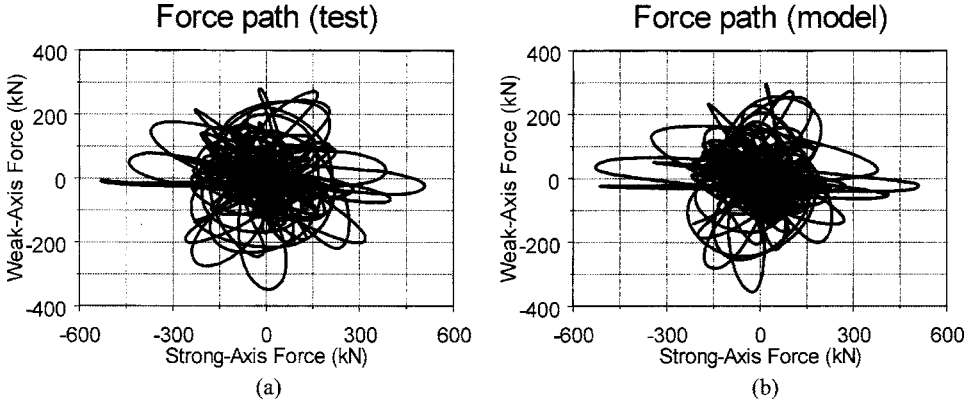

Fig. 12. Force-path orbit under TCU075: (a) test result; (b) model result

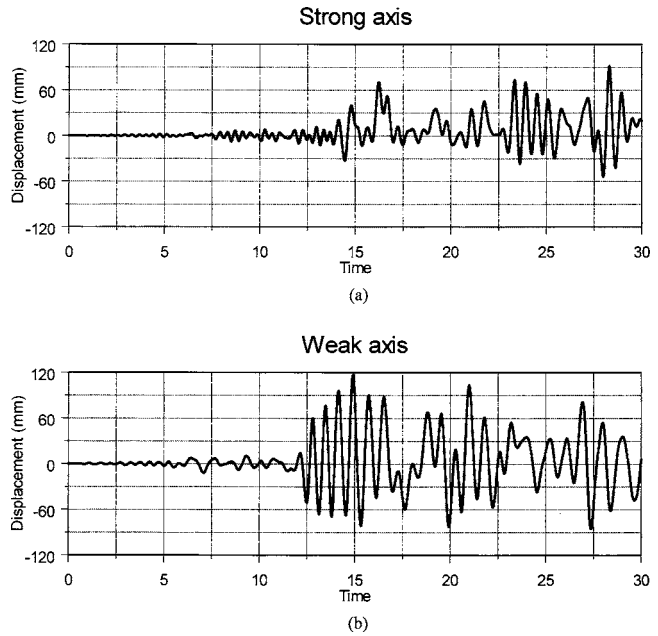

Fig. 13. Pseudodynamic input displacement history using TCU102: (a) strong axis; (b) weak axis

The loading history of the cyclic loading test by Liu (2004) is shown in Fig. 7, in which the ratio of the displacement amplitude in the strong axis to that in the weak axis was maintained as 5:4. The applied axial load was 680 kN, typically used for simulation of a two-lane bridge deck by Taiwan Highway Bureau. First flexural crack was observed when the displacement in the strong axis reached 16 mm, concrete spalled when it reached 50 mm, and longitudinal reinforcements started buckling at 130 mm. At the end of the test, crushed concrete, fractured longitudinal reinforcing bars, and pop-out stirrups were present. Overall, flexure was regarded to be the cause of failures as no significant diagonal shear crack was found (Liu 2004).

Fig. 8(a) shows the hysteresis curves in the strong and weak axes observed from the test. The plots clearly reveal that the specimen underwent slip due to pinching soon after the test started. Severe strength and stiffness degradation occurred after the cyclic displacement reached around 100 mm in the strong axis (or around 80 mm in the weak axis). Fig. 8(b) shows the hysteresis curves obtained from the model by assuming that structural degradation was totally proportional to the cumulative dissipated energy, Eq. (31). The hysteresis behaviors given by the developed model and the cyclic test resemble each other except for the last couple of cycles in the weak axis, in which the test results exhibit lower stiffness and strength than the model results. It may be attributed to buckling of reinforcing bars that occurred right before the last two loading cycles, which caused rapid strength and stiffness degradation. On the other hand, the extent of strength and stiffness degradation in the model results was dictated by energy dissipation which did not subject to similar drastic increase, as observed in the model results. As a further comparison, the lateral force-path orbits from the test and model results are shown in Fig. 9.

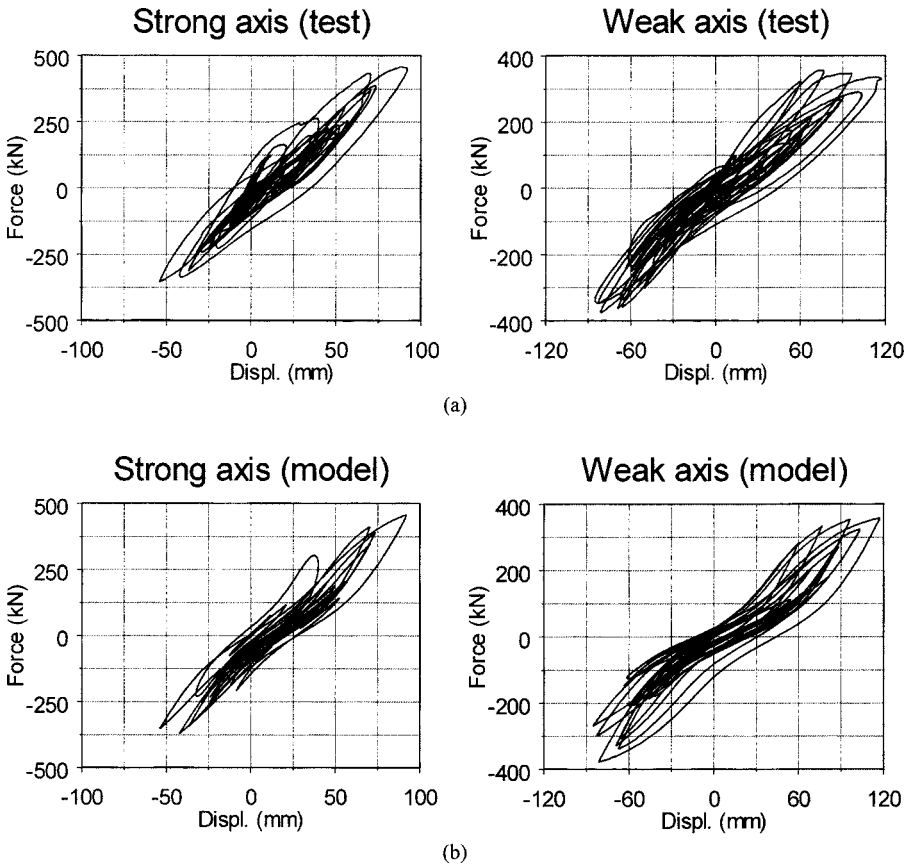

Fig. 14. Hysteresis curves under TCU102: (a) test result; (b) model result

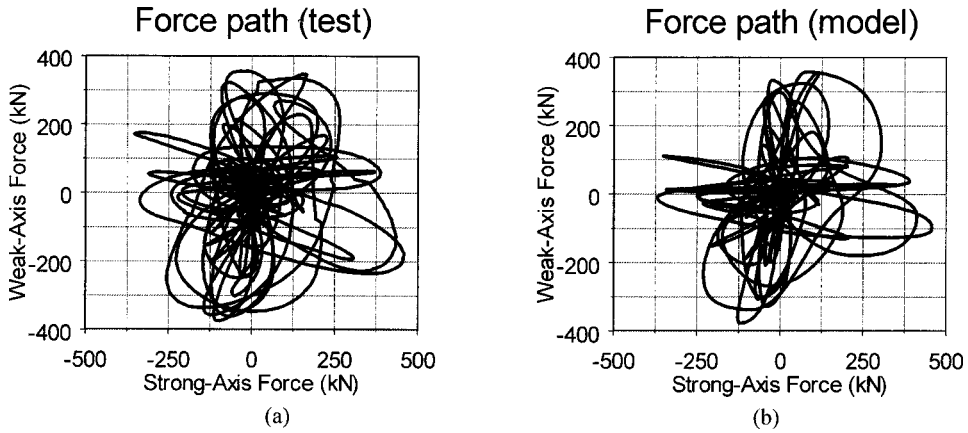

Fig. 15. Force-path orbit under TCU102: (a) test result; (b) model result

Quasi-Static Tests

The two test columns for quasi-static testing (Liu 2004) were subjected to ground motions recorded from the 1999 Chi-Chi Earthquake, Taiwan. One was under the ground motion TCU075, which had an epicentral distance of 19.7 km with peak horizontal ground motions (PGA) of 325 and 257 cm/s^2, respectively, in the east-west (E-W) and north-south (N-S) directions. The other was under TCU102, which had an epicentral distance of 44.33 km with PGA's of 298 and 168.98 cm/s^2, respectively, in the E-W and N-S directions. As with the cyclic test, both columns were subjected to an axial load of 680 kN. For the derivation of simulated results of these two tests, structural degradation was assumed to be due to cumulative energy dissipation only.

To ensure the test column underwent significant inelastic deformation, the ground motion records from TCU075 were scaled such that the PGA's in the E-W and N-S directions were 800 and 630 cm/s^2, respectively. The E-W component was applied to the strong axis and the N-S component to the weak axis of the column. The displacement history is shown in Fig. 10. At the end of testing, longitudinal reinforcement yielding was detected but no bucking observed. Flexural cracks and concrete cover spalling around the corners occurred. In general, the test column suffered minor damage only and performed satisfactorily.

Hysteresis curves obtained from this test about the strong and weak axes are plotted in Fig. 11(a), which shows apparent stiffness degradation and spread of pinching but no obvious strength degradation as the maximum forces had not been close to the strength limits. The hysteresis in the strong axis also had larger spread of pinching than that in the weak axis.

The model results are shown in Fig. 11(b). Since the hysteretic parameter values were chosen to obtain a better fitting to the weak-axis hysteresis, the most obvious discrepancy for the strong-axis hysteresis between test and model results is that modeled hysteresis has a much less pinching spread. The force-path orbits are shown in Fig. 12.

For the test under the ground motion TCU102, the ground motion records were scaled to the PGA values of 500 and 280 cm/s^2 in the E-W and N-S directions, respectively. The E-W component was applied to the strong axis and the N-S component to the weak axis. The displacement history is shown in Fig. 13. Though the PGA's of the scaled TCU102 are smaller than that of the scaled TCU075, its peak resultant displacement is 120 mm, as opposed to 89 mm for the scaled TCU075. At the end of testing, flexural cracks and severe concrete cover spalling occurred. In addition, longitudinal reinforcement yielding was detected and some of them were slightly buckled. Overall, this specimen suffered more damage than the one under TCU075.

Hysteresis curves obtained from this test about the strong and weak axes are plotted in Fig. 14(a). Both curves exhibit a sudden slip of pinching when the displacement in the positive direction

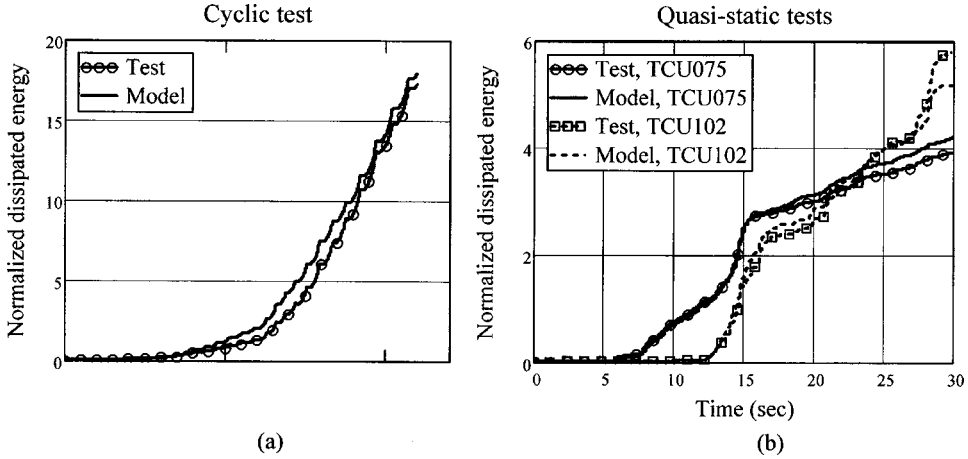

Fig. 16. Normalized dissipated energy: (a) cyclic test by Liu (2004); (b) quasi-static tests

of the strong axis exceeds 40 mm but limited spread of pinching afterward. The strong-axis hysteresis, however, indicates no apparent strength and stiffness deterioration, whereas the weak-axis hysteresis reveals the opposite.

The simulated hysteresis curves are shown in Fig. 14(b). Compared to the test results, the obvious discrepancy between them is the spread of pinching, which in the model is considered via accumulated energy dissipation. Since energy dissipation is only accumulated gradually, it is unable to capture a sudden increase of slip as observed in the test results. Other damage measures allowing sudden increase of deterioration are needed to get better simulated results. The force-path orbits are shown in Fig. 15.

Note that in Table 2 different positive and negative yield forces for the specimens under TCU075 and TCU102 are used, meaning that the hysteresis curves were regarded as asymmetric.

Energy Dissipation

The validity of the developed model is further demonstrated in energy dissipation. Fig. 16 shows the normalized dissipated energies of the specimens by Liu (2004) and by the model. At the end of the cyclic test, the model overestimates the dissipated energy slightly by 4%, whereas it overestimates by 7% for the specimen under TCU075 and underestimates by 10% for the specimen under TCU102. Over the entire test histories of the three cases, the estimated dissipated energies are reasonably close to the test results, apart from the last couple of cycles of the test under TCU102, where a dramatic divergence occurs. This may be attributed to the fact that the TCU102 specimen experienced more severe cumulative damages at the end of the test than the other specimens.

Summary and Conclusions

Based on the model by Park et al. (1986), this paper presents a generalized biaxial hysteresis model that takes into account the commonly observed hysteretic characteristics such as the asymmetry in yield strength, strength and/or stiffness degradation, pinching, negative stiffness, and rounded corners. While the model was validated by using RC-column test data only, it may be applied to other types of construction, for example, steel and composite materials, given its versatility in modeling a wide range of hysteretic behavior.

Since the developed model is in the category of concentrated plasticity, it serves the most effectively when used in modeling the behavior of flexure-dominated structural members with concentrated inelastic regions, particularly those with inelasticity concentrated at the two ends. Though not explicitly given in this paper, the effect of axial-flexural force interaction on the yield moments may be accommodated by using a properly constructed three-dimensional yield surface. If excessive axial load exists or the structural element is subjected to large lateral displacement, geometric nonlinearity may need to be considered in tandem with application of the model.

As with most analytical models, the developed model assumes that the system is perfectly orthotropic, ductile with gradual degradation dependent on the degradation parameters chosen, whereas it often happens in practical situations, particularly for reinforced concrete structures, that a system is inhomogeneous and brittle failure could occur if not designed or constructed properly. Extension of the model to take into account sudden brittle failure is warranted in future work. Another possible extension of the model is to allow different hysteretic parameter values in the two orthogonal directions so that different hysteretic properties; e.g., spread of pinching and the rate of strength/stiffness degradation as observed from the test results investigated in this study, could be more accurately considered.

Acknowledgments

The first writer is grateful for the support of this collaborative study by the Australian Academy of Science under an international scientific collaboration program RI-82-03/04.

References

Abrams, D. P. (1987a). "Influence of axial force variation on flexural behavior of reinforced concrete columns." *ACI Struct. J.*, 84(3), 246–254.

Abrams, D. P. (1987b). "Scale relations for reinforced concrete beam-column joints." *ACI Struct. J.*, 84(6), 502–512.

Aktan, A. E., and Pecknold, D. A. (1974). "Response of a reinforced concrete section to two-dimensional curvature histories." *J. Am. Concr. Inst.*, 71(5), 246–250.

Baber, T. T., and Noori, M. N. (1985). "Random vibration of degrading, pinching systems." *J. Eng. Mech.*, 111(8), 1010–1026.

Bockstedte, A. (1999). "Model adjustment to parameter identification of hysteretic structures." *Project Rep.*, Advisor F. Ma, Dept. of Mechanical Engineering, Univ. of California, Berkeley, Calif.

Bousias, S. N., Verzeletti, G., Fardis, M. N., and Gutierrez, E. (1995). "Load-path effects in column biaxial bending with axial force." *J. Eng. Mech.*, 121(5), 596–605.

Bresler, B. (1960). "Design criteria for reinforced concrete columns under axial load and biaxial bending." *J. Am. Concr. Inst.*, 57(11), 481–490.

Cheng, F. Y. (2001). *Matrix analysis of structural dynamic: Applications and earthquake engineering*, Marcel Dekker, New York.

El-Tawil, S., and Deierlein, G. G. (200la). "Nonlinear analysis of mixed steel-concrete frames. I: Element formulation." *J. Struct. Eng.*, 127(6), 647–655.

El-Tawil, S. and Deierlein, G. G. (2001b). "Nonlinear analysis of mixed steel-concrete frames. II: Implementation and verification." *J. Struct. Eng.*, 127(6), 656–665.

Fajfar, P. (1992). "Equivalent ductility factors, taking into account low-cycle fatigue." *Earthquake Eng. Struct. Dyn.*, 21, 837–848.

Furlong, R. W., Hsu, C-T. T., and Mirze, S. A. (2004). "Analysis and design of concrete columns for biaxial bending—Overview." *ACI Struct. J.*, 101(3), 413–423.

Goto, Y., Wang, Q., and Obata, M. (1998). "FEM analysis for hysteretic behavior of thin-walled steel columns." *J. Struct. Eng.*, 124(11), 1290–1301.

Jiang, L., Goto, Y., and Obata, M. (2002). "Hysteretic modeling of thin-walled circular steel columns under biaxial bending." *J. Struct. Eng.*, 128(3), 319–327.

Japanese Society of Civil Engineers. (JSCE). (1995). "Preliminary report on the Great Hanshin Earthquake, January 17, 1995."

Kunnath, S. K., and Reinhorn, A. M. (1990). "Model for inelastic biaxial bending interaction of reinforced concrete beam-columns." *ACI Struct. J.*, 87(3), 284–291.

Lai, S. S., and Will, G. T. (1986). "R/C space frames with column axial force and biaxial bending moment interactions." *J. Struct. Eng.*, 112(7), 1553–1572.

Li, S. J., Suzuki, Y., and Noori, M. (2004). "Improvement of parameter estimation for non-linear hysteretic systems with slip by a fast Bayesian Bootstrap filter." *Int. J. Non-Linear Mech.*, 39(9), 1435–1445.

Liu, L-C. (2004). "Simulations of seismic responses of reinforced concrete bridge columns." Master's thesis, Advisor S-Y. Chang,

NTUT-91428005, Dept. of Civil Engineering, National Taipei Univ. of Technology, Taipei, Taiwan, R.O.C.

Ma, F., Zhang, H., Bockstedte, A., Foliente, G. C., and Paevere, P. (2004). "Parameter analysis of the differential model of hysteresis." *J. Appl. Mech.*, 71(3), 342–349.

Marante, M. E., and Flórez-López, J. (2002). "Model of damage for RC elements subjected to biaxial bending." *Eng. Struct.*, 24, 1141–1152.

Marante, M. E., and Flórez-López, J. (2003). "Three-dimensional analysis of reinforced concrete frames based on lumped damage mechanics." *Int. J. Solids Struct.*, 40, 5109–5123.

McGuire, W., Gallagher, R. H., and Ziemian, R. D. (2000). *Matrix structural analysis*, 2nd Ed., Wiley, New York.

Mostaghel, N. (1999). "Analytical description of pinching, degrading hysteretic systems." *J. Struct. Eng.*, 125(2), 216–224.

Paevere, P., and Foliente, G. C. (2000). "Hysteretic pinching and degradation effects on dynamic response." *Proc., ICASP 8, Applications of Statistics and Probability*, Melchers and Stewart, eds., Balkema, Rotterdam, 771–779.

Park, Y. J., and Ang, A.H-S. (1985). "Mechanistic seismic damage model for reinforced concrete." *J. Struct. Eng.*, 111(4), 722–739.

Park, Y. J., Wen, Y. K., and Ang, A.H-S. (1986). "Random vibration of hysteretic systems under bi-directional ground motions." *Earthquake Eng. Struct. Dyn.*, 14, 543–557.

Press, W. H., Teukolsky, S. A., Vetterling, W. T., and Flannery, B. P. (1992). *Numerical recipes in Fortran 77: The art of scientific computing*, 2nd Ed., Cambridge Univ., Cambridge, England.

Qiu, F., Li, W., Pan, P., and Qian, J. (2002). "Experimental tests on reinforced concrete columns under biaxial quasi-static loading." *Eng. Struct.*, 24, 419–428.

Sivaselvan, M. V., and Reinhorn, A. M. (2000). "Hysteretic models for deteriorating inelastic structures." *J. Eng. Mech.*, 126(6), 633–640.

Suharwardy, M. I. H., and Pecknold, D. A. (1978). "Inelastic response of reinforced concrete columns subjected to two-dimensional earthquake motions." Civ. Eng. Studies, *Struct. Res. Series No. 455*, Univ. of Illinois, Urbana, Ill.

Takizawa, H., and Aoyama, H. (1976). "Biaxial effects in modeling earthquake response of R/C structures." *Earthquake Eng. Struct. Dyn.*, 4, 523–552.

Wang, C-H., and Foliente, G. C. (2000). "Building damage and lessons learned from the Taiwan Chi-Chi Earthquake of 21 September 1999." BCE Doc 99/228, CSIRO Manufacturing and Infrastructure Technology, Melbourne, Australia.

Wang, C-H., and Foliente, G. C. (2006). "Seismic reliability of low-rise nonsymmetric woodframe buildings." *J. Struct. Eng.*, 132(5), 733–744.

Wang, C-H., and Wen, Y. K. (1998a). "Redundancy of steel frame buildings under seismic loads." *ICOSSAR'97*, Shiraishi, Shinozuka, and Wen, eds., Balkema, Rotterdam, 1645–1652.

Wang, C-H., and Wen, Y. K. (1998b). "Reliability and redundancy of pre-Northridge low-rise steel buildings under seismic excitation." Civ. Eng. Studies, *Struct. Res. Series No. 624*, Dept. of Civ. and Environ. Eng., Univ. of Illinois, Urbana, Ill.

Wang, C-H., and Wen, Y. K. (2000). "Evaluation of pre-Northridge low-rise steel buildings. I: Modeling." *J. Struct. Eng.*, 126(10), 1160–1168.

Wen, Y. K. (1976). "Method for random vibration of hysteretic systems." *J. Engrg. Mech. Div.*, 102(2), 249–263.

Wen, Y. K., and Yeh, C. H. (1989). "Biaxial and torsional response of inelastic structures under random excitation." *Struct. Safety*, 6, 137–152.

Wilson, E. L., and Habibullah, A. (1987). "Static and dynamic analysis of multi-story building, including P–Δ effects." *Earthquake Spectra*, 3(2), 289–298.

Yang, Y-B., and Kuo, S-R. (1994). *Theory and analysis of nonlinear framed structures*, Prentice-Hall, Englewood Cliffs, N.J.

Zahn, F. A., Park, R., and Priestley, M. J. N. (1989). "Strength and ductility of square reinforced concrete column sections subjected to biaxial bending." *ACI Struct. J.*, 56(2), 123–130.